Electron band model of bismuth by magnetic surface resonance

S. Takaoka, H. Kawamura, K. Murase, and S. Takano*
Department of Physics, Osaka University, Toyonaka, 560 Japan
(Received 19 May 1975; revised manuscript received 6 October 1975)

The magnetic-field-induced surface-state resonance of bismuth was measured for the surface parallel to the binary plane. From the observed resonance signal, we could obtain information on the Fermi surface of electrons along the equator parallel to the binary plane. It was found that the spectra near the heavy-mass direction can neither be interpreted with the band model by Lax nor with that by Cohen. They were explained satisfactorily with a "hybrid" model in which both the two-band coupling and the remote-band effect are taken into account in the heavy-mass direction.

I. INTRODUCTION

The band structure and Fermi surface of electrons in bismuth have been studied by various experimental methods: Azbel-Kaner cyclotron resonance,[1-3] Shubnikov–de Haas effect,[4] de Haas–van Alphen effect,[5,6] giant quantum attenuation,[7] geometric resonance of acoustic waves,[8,9] radio-frequency size effect,[10] cutoff of cyclotron orbit,[11] magneto-optical reflection,[12-14] and Alfvén wave interference.[15-17] These experimental results were interpreted with the simple two-band model due to Lax *et al.*[12] which gives rise to the ellipsoidal Fermi surface with nonparabolic bands, or with the modified two-band model by Cohen giving the nonellipsoidal Fermi surface and nonparabolic bands.[18] The above methods, however, are not necessarily adequate to investigate the detailed band structures near the heavy-mass direction on the Fermi surface. From the Shubnikov–de Haas, de Haas–van Alphen, or giant quantum attenuation effect, we can only measure the cross-sectional area of the Fermi surface. The cyclotron mass of the extremal orbit determined from Azbel-Kaner resonance also reflects the average nature of the Fermi surface. It may be useful to get the limiting point mass by Azbel-Kaner resonance, but practically it is very difficult to measure because of the rigorous alignment of the experimental configuration.[1] The geometric resonance of acoustic waves, radio-frequency size effect, or cutoff of cyclotron orbit caliper the Fermi surface. However, the shape of the Fermi surface is insensitive to the nonparabolicity of the band structure. As shown in the following, the magnetic-field-induced surface-state resonance gives a direct information on the curvature and the Fermi velocity at a particular point on the Fermi surface. We found that both the Lax model and the Cohen model do not fit our observations. We could interpret our results satisfactorily with a "hybrid" of the Lax model and the Cohen model.

II. ELECTRON BAND STRUCTURE OF BISMUTH

The minima of the conduction band of bismuth are at L points in the Brillouin zone. One of the Fermi surfaces of electrons is a pseudoellipsoid with the major axis pointing along the direction tilted from the bisectrix axis to the trigonal axis by $6°20'$[1] as shown in Fig. 1. The mass parameters in the parabolic approximation are $m_1^* = 0.0059m_0$, $m_2^* = 1.304m_0$, and $m_3^* = 0.011m_0$,[1] the principal axes being denoted as 1, 2, and 3 as shown in the figure. Two equivalent Fermi surfaces are obtained by rotations of $\pm 120°$, about the trigonal axis. Just 13.5 meV below each band minimum,[14] there is a valence-band maximum. According to the spirit of $\vec{k}\cdot\vec{p}$ perturbation by Kane,[19] the coupling between these closely spaced levels gives rise to the repulsion of the energy levels at the off-symmetry points in the Brillouin zone (two-band theory). The general two-band theory, where the effect from remote bands is also taken into account as perturbations, gives the energy-dispersion relation[18]

$$(E - \tfrac{1}{2}\vec{p}\circ\overleftrightarrow{M}'^{-1}\cdot\vec{p})(E + E_g + \tfrac{1}{2}\vec{p}\circ\overleftrightarrow{M}^{-1}\cdot\vec{p}) = \tfrac{1}{2}E_g\vec{p}\circ\overleftrightarrow{m}^{-1}\cdot\vec{p}, \quad (1)$$

where E_g is the energy gap and $\overleftrightarrow{M}^{-1}$ and $\overleftrightarrow{M}'^{-1}$ are the inverse mass tensors of the conduction band and valence band, respectively, contributed from remote bands, and $\overleftrightarrow{m}^{-1}$ is the inverse mass tensor due to the coupling between conduction band and valence band.

Since in the case of bismuth, the two-band couplings in the directions of the 1 and 3 axes are much stronger than those with remote bands, it is good approximation to neglect M_1^{-1}, M_2^{-1}, $M_1'^{-1}$, and $M_2'^{-1}$ in Eq. (1). By this approximation, Eq. (1) is reduced to be

$$(E - P_2^2/2M_2')(E + E_g + P_2^2/2M_2) = \tfrac{1}{2}E_g\vec{p}\cdot\overleftrightarrow{m}^{-1}\cdot\vec{p}. \quad (2)$$

If the effects from all the remote bands are ne-

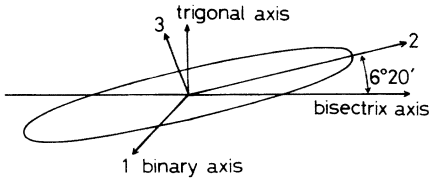

FIG. 1. Schematic drawing of a Fermi surface of electrons in bismuth.

glected, we get the Lax model[12]

$$E(E+E_g)=\tfrac{1}{2}E_g\vec{p}\cdot\overleftrightarrow{m}^{-1}\cdot\vec{p}. \tag{3}$$

This dispersion relation gives an ellipsoidal Fermi surface with nonparabolic dispersion. On the other hand, if the two-band coupling in the direction of two axis is neglected, Eq. (2) is reduced to the Cohen model[18]

$$(E-p_2^2/2M_2')(E+E_g+p_2^2/2M_2)$$
$$=E_g(p_1^2/2m_1+p_3^2/2m_3)\,. \tag{4}$$

The dispersion relation (4) results a nonellipsoidal Fermi surface as well as a nonparabolic dispersion.

III. MAGNETIC SURFACE LEVELS

With the magnetic field H applied parallel to the surface of a metal, electrons running almost parallel to the surface undergo the Lorentz force $(e/c)\,Hv_\perp$ perpendicular to the surface, where $v_\perp$ is the velocity of the electron perpendicular to the magnetic field. The electrons are trapped one dimensionally at the surface quantum level by a nearly triangular potential well due to this force.[20,21] The oscillating electric field polarized in the plane of the surface and perpendicular to the magnetic field gives rise to the transitions between these quantum levels conserving the momenta along the surface. The most characteristic feature is that the energy levels in the direction perpendicular to the surface are determined by the quite local behaviors on the Fermi surface as

$$E_n=\hbar(eH/cH)^{2/3}(v_F^3/\kappa_F)_\perp^{1/3}a_n\,, \tag{5}$$

where $a_n=[\frac{3}{2}\pi(n-\frac{1}{4})]^{2/3}$, $n=1,\ 2,\ \ldots$. As shown in Fig. 2, the Fermi velocity v_F and the radius of curvature κ_F are associated with the segment of the extremal orbit on the equator parallel to the sample surface where the velocity component normal to the surface vanishes.[22] The resonant magnetic field for the transition from nth state to mth state by the oscillating electric field with frequency ω is given by

$$H_{nm}=(c\hbar/e)\,(2\kappa_F/v_F^3)_\perp^{1/2}[\omega/(a_n-a_m)]^{3/2}. \tag{6}$$

A lot of work on the magnetic-field-induced surface-state resonance has been performed for various metals and semimetals including bismuth, in order to investigate the Fermi surface and band structure. For bismuth, Koch and Jensen[22] and Khaikin[23] have made detailed studies for the determination of the electron-band structure. Their investigations were limited in the central cross section with the smallest cyclotron mass (1-3 plane). They found that the ellipsoidal model holds fairly well. However, a serious deviation from the simple elliposidal model is expected in the direction of the major axis (axis 2, see Fig. 1). We have measured the angular dependence of the resonance spectra with the magnetic field in the binary plane (2-3 plane) and examined the validity of the various band models.

IV. EXPERIMENTAL

The magnetic-field-induced surface-state resonance was observed as an oscillatory variation with magnetic field of the microwave impedance of clean surface of a sample. The microwave reflection-type spectrometer was operated at 35 GHz. The specimens were fixed at the end of a cylindrical cavity resonator, operated in the TE_{113} mode. The microwave frequency was stabilized with an automatic frequency-control system referred to the sample cavity with Q value of about 100 00 at liquid-helium temperature. A magnetic field up to 400 G was produced with a pair of Helmholtz coils. The field intensity was calibrated with an ESR signal from a 2, 2-diphenyl-1-picrylhydrazyl sample at several hundred MHz. The measurements were performed at 1.8 and 4.2 K.

The single crystal of bismuth was prepared by zone refining for 30 times starting from the six-nine material supplied by Osaka Asahi Metal Inc.. The single crystal was cut in a trigonal plane or in a binary plane. The treatment of the sample surface is most important for this experiment. We followed the prescription given by Koch and Jensen.[22] The binary plane was more difficult to finish than the trigonal plane.

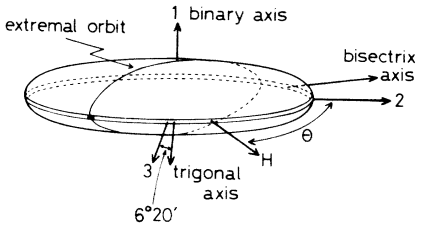

FIG. 2. Local point on the electron Fermi surface, which is responsible for the magnetic-field-induced surface-state resonance.

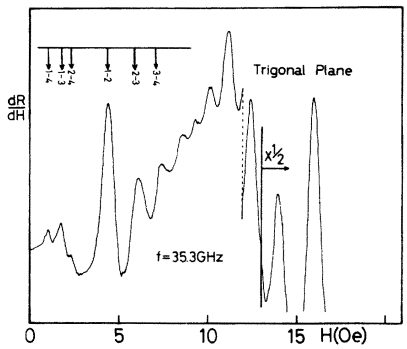

FIG. 3. Magnetic-field derivative of the real part of the surface impedance as a function of magnetic field. The surface of the sample is parallel to the trigonal axis and the magnetic field is parallel to a bisectric axis. The arrows are the positions of the magnetic-field-induced surface-state resonance of electrons (see text).

V. EXPERIMENTAL RESULTS AND DISCUSSIONS

In Fig. 3, typical data for the magnetic-field derivative of the reflection signal are shown for the specimen with trigonal surface and magnetic field parallel to a bisectric axis. The arrows in the figure are the positions of the resonances determined from Eq. (6) with $m_1^* = 0.0059 m_0$,[1] $p_1 = 0.545 \times 10^{-21}$ g cm/sec, and $p_2 = 0.76 \times 10^{-21}$ g cm/sec.[8,10]

Figure 4 shows the spectra for the specimen with binary plane surface. The magnetic field was rotated from the two axis (0°) to the three axis (90°). Although, the microwave current is nearly along the two direction on the surface, we can observe the signal from the point of the three axis on the Fermi surface even with the magnetic field parallel to the two axis. This is because a small bend of the microwave field causes excitation of the electrons running along the three axis. In Fig. 4, we observe only the signals from the valley nearly parallel to the bisectrix axis. For a magnetic field nearly parallel to the two axis, other valleys give signals at higher field, which will be buried in the Azbel-Kaner signal. In Fig. 5, the main peak which corresponds to H_{21} is plotted as a function of tilt angles of the magnetic field against the two axis.

In order to explain the results shown in Fig. 5, we have to calculate the values $2\kappa_\perp/v_\perp^3 = Y$ shown in Eq. (6) based on the proposed band models. We shall rewrite Eq. (2)

$$E(1+\lambda) - \beta p_2^2/2M_2 - \gamma p_2^4/4M_2^2 E_g = p_1^2/2m_1 + p_3^2/2m_3 , \tag{7}$$

where

$$\gamma = M_2/M_2', \quad \delta = M_2/m_2, \quad \lambda = E/E_g ,$$

and

$$\beta = 1 + \lambda - \lambda\gamma + \delta .$$

With this notation, the value of Y in the cross section of the 2-3 plane under the magnetic field with the tilt angle θ from two axis is given by

$$Y = \frac{m_1 m_3^2 \tan^2\theta(1+\tan^2\theta)[(1+2\lambda)+(\gamma-1)W]^3}{M_2 E_g W[1+(m_3/M_2)\tan^2\theta(\beta+2\gamma W)]^2} , \tag{8}$$

where

$$W = (1/\gamma\tan^2\theta)\{-\tfrac{1}{2}(\beta\tan^2\theta + M_2/m_3) + [\tfrac{1}{4}(\beta\tan^2\theta + M_2/m_3)^2 + \lambda\gamma(\lambda+1)\tan^4\theta]^{1/2}\} .$$

For the Lax model, taking $\delta \to \infty$, we get

$$Y = \frac{m_1 m_3 (1+2\lambda)^3 (1+\tan^2\theta)}{E(1+\lambda)[1+(m_3/m_2)\tan^2\theta]} . \tag{9}$$

The Cohen model is obtained by putting $\delta = 0$.

The cyclotron masses for the three principal orbits are given by

$$m_{c1} = (m_2^* m_3^*)^{1/2}, \quad m_{c2} = (m_1^* m_3^*)^{1/2},$$

and

$$m_{c3} = (m_1^* m_3^*)^{1/2} , \tag{10}$$

where m_1^*, m_2^*, and m_3^* are the effective masses in the principal axes on the Fermi surface in the parabolic approximation. If the expressions for cyclotron masses based on the nonparabolic dispersion relation (7) are put equal to Eq. (10), we have

$$M_2 = m_2^* \left(\frac{\pi\gamma}{2\gamma(1+2\lambda)K(k) + (1-\gamma)[(\beta+\sqrt{z})K(k) - 2\sqrt{z}E(k)]} \right)^2 \sqrt{z}(1+2\lambda) , \tag{11a}$$

$$m_1 = m_1^*/(1+2\lambda) , \tag{11b}$$

$$m_3 = m_3^*/(1+2\lambda) , \tag{11c}$$

where

$$z = \beta^2 + 4\gamma\lambda(\lambda+1) ,$$

$$k^2 = (-\beta+\sqrt{z})/2\sqrt{z} ,$$

and $K(k)$ and $E(k)$ are the complete elliptic integral of first and second kind, respectively. In Eq. (11a) the parameters M_2' and m_2 are also included through γ and β. For the Cohen model, Eqs. (11) become[24]

$$M_2 = (\tfrac{1}{2}\pi)^2 \frac{\gamma^2(1+2\lambda)m_2^*}{(1+\lambda+\lambda\gamma)[K(k)+(\gamma-1)E(k)]^2} , \tag{12a}$$

$$m_1 = m_1^*/(1+2\lambda), \tag{12b}$$

$$m_3 = m_3^*/(1+2\lambda), \tag{12c}$$

where

$$k^2 = \gamma\lambda/(1+\lambda+\lambda\gamma).$$

For the Lax model the relations are simply given by

$$m_i = m_i^*(1+2\lambda), \quad i=1,\ 2,\ 3, \tag{13}$$

for all masses.

For the parabolic effective-mass tensor components, we employed the following values which were determined from Azbel-Kaner resonance by Edel'man *et al.*[1]

$$m_1^* = 0.059m_0, \quad m_2^* = 1.304m_0, \quad m_3^* = 0.011m_0. \tag{14}$$

The value of $\lambda = E/E_g$ can be obtained from $E_g = 13.5$ meV determined by Vicchi *et al.*[14] and from the value of Y at $\theta = 0°$, which is given by

$$Y = m_1 m_3 (1+2\lambda)^3/E(1+\lambda), \tag{15}$$

independent of the above models. Using the experimental value $H_{12} = 9.149\times10^{22}\sqrt{Y} = 4.0$ Oe and the above value of E_g, we get $\lambda = E/E_g = 2.2$.

For the Lax model, the parameters are m_1, m_2, m_3, and λ. The values of m_1, m_2, and m_3 are determined by (13) and (14). Putting these parameters and $\lambda = 2.2$ into Eq. (9), we get a curve shown in Fig. 5(a). The theoretical values are about 15% larger than the experimental values at the vicinity of 90°. In the case of the Cohen model, the parameters M_2/M_2' can not be uniquely determined from the Eqs. (12) with the value of $\lambda = 2.2$. We took $\gamma = 3.2$ to fit the experimental and theoret-

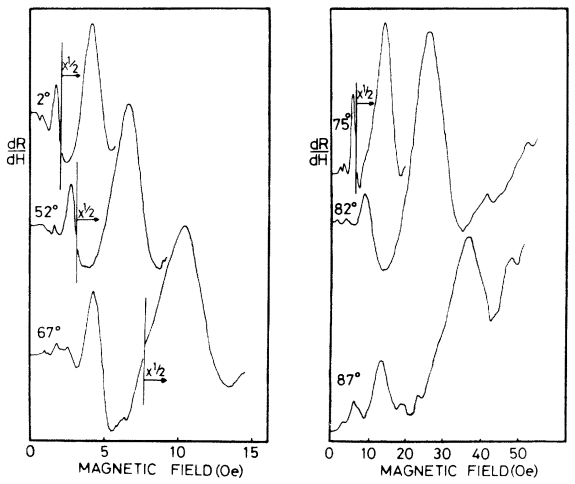

FIG. 4. Magnetic-field-induced surface-state resonance spectra for the sample with binary plane surface. The magnetic field is rotated from the two axis (0°) to the three axis (90°).

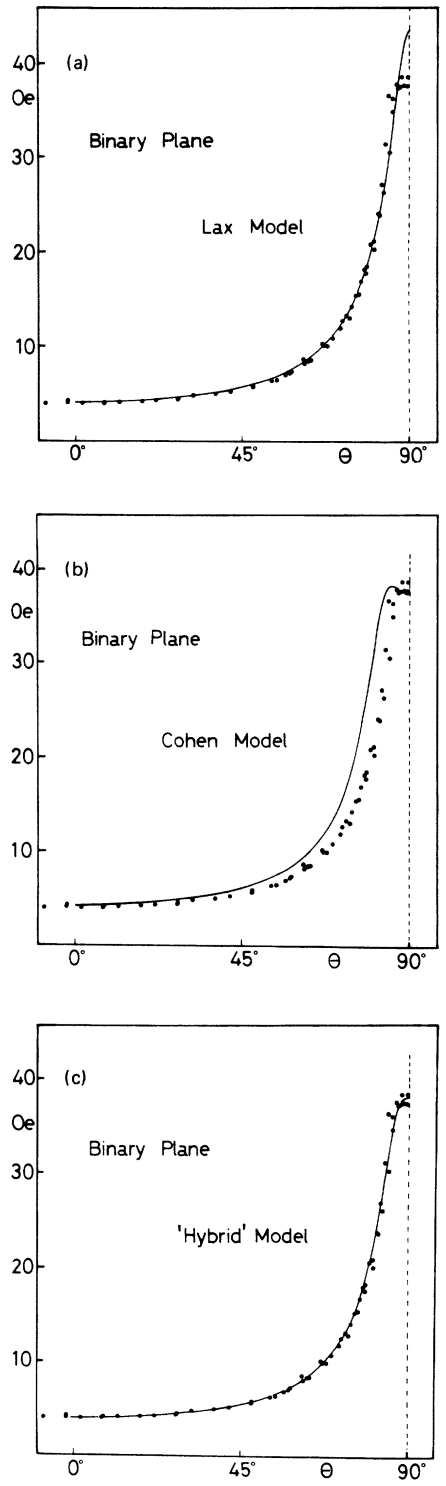

FIG. 5. Magnetic field (H_{21}) corresponding to the resonant excitations from the ground state to the first excited state as a function of angle between the magnetic field and the two axis in the plane normal to the one axis. The solid circles are the experimental points and the lines are the theoretical based on the Lax model (a), the Cohen model (b), and the present model (c).

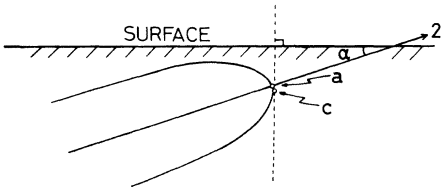

FIG. 6. Enlarged sketch near the point of the two direction on the Fermi surface of electrons. If the surface on the sample is tilted, the resonance signal comes from the point "c" instead of the point "a."

ical values at 90°. The theoretical curve with these parameters are shown in Fig. 5(b). The disagreements are remarkable between 60° and 80°.

It is more realistic to take into account the two-band coupling and the perturbation from the remote bands on an equal footing, in the direction of the two axis where the effective mass is of the same order with the free mass. This model which is a "hybrid" of the Lax model and the Cohen model, contains another parameter $\delta = M_2/m_2$, as shown in Eq. (2). Using $\lambda = E/E_g = 2.2$, $\gamma = M_2/M_2' = 1.6$, and $\delta = M_2/m_2 = 3.2$, with the mass parameters in (14), we have the theoretical curve with very good agreement with experiment as shown in Fig. 5(c).

It should be mentioned that these conclusions are not altered considerably so far as E_g is less than 20 meV, although the parameters γ and δ change a little, with a small change of E_g.

In the process of the sample preparation, the surface of the sample deviates from the binary plane less than 3°. For $\theta = 0°$, the misorientation of angle 3° shifts the peak position by the factor of $1/\cos 3° = 1.001$. The magnetic surface level

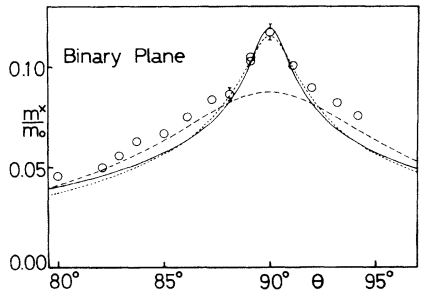

FIG. 7. Angular variation of the limiting-point cyclotron mass near the three axis for magnetic field in the binary plane. The experimental points are due to Edel'man *et al.* (Ref. 1). The solid line is computed from the present model with the same parameters as used in Fig. 5(c), the dotted line from the Cohen model with $\lambda = 0.5$, and the broken line from the Lax model.

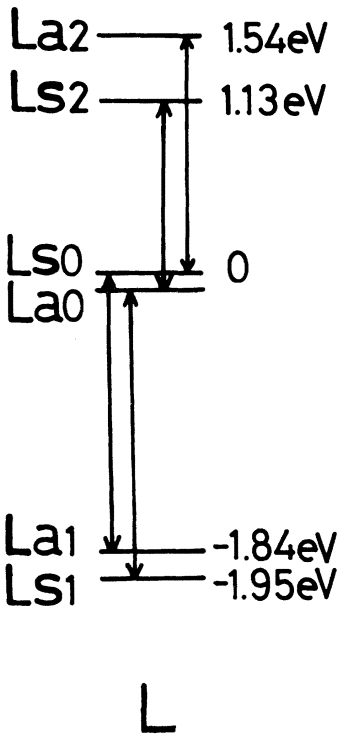

FIG. 8. Electron energy-level diagram of bismuth at the L point. The conduction band L_{s0} couples with L_{a1} and L_{a2}, and the valence band L_{a0} couples with L_{s1} and L_{s2}.

for $\theta = 90°$ comes from the point "c" shown in Fig. 6, when the surface is tilted. Since the anisotropy factor of the Fermi surface is as large as 100, the point "c" can not be distinguished from the point of the Fermi surface "a".

Dinger and Lawson[24] have tried to fit the limiting-point cyclotron mass near the three axis, measured by Edel'man and Khaikin,[1] with the Cohen model. They obtained an agreement between experiments and the theory with $\lambda = 0.5$, which requires an unrealistically large value of the energy gap (47 meV). The present model with the above parameters gives a better fitting with experimental points than the Cohen model as shown in Fig. 7.

In Table I are shown the electronic band parameters for the Lax model and the Cohen model, as well as the present model. For the Cohen model, the cases for both $E_g = 13.5$ meV ($\lambda = 2.2$, case I) and 47 meV ($\lambda = 0.5$, case II) are shown. All sets of parameters are chosen so that the cyclotron masses for extremum orbit should be consistent with Eq. (14). On the other hand, the cyclotron masses at the limiting points are different for different models. The Cohen model II and the present model give good fits with the experiment as shown in the table. However, it should be mentioned that a recent experiment[14] clearly shows

TABLE I. Electronic band parameters for the Lax model, the Cohen model, and the present model.

	E_g (meV)	E_F (meV)	m_1	m_2	m_3	M_2	M_2'	Cyclotron mass at limiting point m_{c1}^*	m_{c2}^*	m_{c3}^*
Present model ($\lambda = 2.2$, $\gamma = 1.6$, $\delta = 3.2$)	13.5	29.7	0.00109	0.401	0.00204	1.28	0.80	0.158	0.0093	0.119
Lax model ($\lambda = 2.2$)	13.5	29.7	0.00109	0.241	0.00204			0.120	0.0081	0.88
Cohen model I ($\lambda = 2.2$, $\gamma = 3.2$)	13.5	29.7	0.00109		0.00204	0.75	0.24	0.108	0.0153	0.079
Cohen model II ($\lambda = 0.5$, $\gamma = 1.0$)	47	23.5	0.00295		0.0055	1.13	1.13	0.155	0.0081	0.116
					Experiment (Ref. 1)			0.137		0.117

that 13.5 meV rather than 47 meV is better for the value of E_g.

The inverse mass parameters $1/M_2$ and $1/M_2'$ are given by

$$\pm\left(\frac{1}{m}+2\sum_{i\neq 0}\frac{|\langle 0|p_2|i\rangle|^2}{E_0-E_i}\right), \tag{16}$$

where the "+" sign is for $1/M_2$ and the "−" sign for $1/M_2'$, respectively, p_2 is the momentum operator in the two direction, and 0 and i show the conduction or valence band, and the other remote bands at the L point, respectively. The energy-level diagram at the L point is shown in Fig. 8,[25] where L_{s0} and L_{a0} are the conduction and valence band, respectively. The L_s and L_a levels can couple to each other. The coupling of L_{s0} with L_{a1} and L_{a2} gives rise to the deviation of M_2 from the free-electron mass m.

VI. CONCLUSION

The magnetic-field-induced surface-state resonance was observed on the surface of the binary plane in bismuth. The Fermi surface and energy dispersion relation of the electron were investigated on the central cross section perpendicular to the binary axis. The results can neither be interpreted satisfactorily by the Lax model nor by the Cohen model. Instead, we have proposed a "hybrid" model in which both the two-band coupling and the remote-band effect are taken into account on equal footing in the heavy-mass direction.

*Present Address: Dept. of Physics, Kyushu University, Hakozaki, Fukuoka, 812 Japan.

[1]V. S. Edel'man and M. S. Khaikin, Zh. Eksp. Teor. Fiz. 49, 107 (1965) [Sov. Phys.-JETP 22, 77 (1966)].
[2]Y. H. Kao, Phys. Rev. 129, 1122 (1963).
[3]R. J. Dinger and A. W. Lawson, Phys. Rev. B 7, 5215 (1973).
[4]R. J. Balcombe and A. M. Forrest, Phys. Rev. 151, 550 (1966).
[5]R. N. Bhargava, Phys. Rev. 156, 785 (1967).
[6]V. S. Edel'man, Zh. Eksp. Teor. Fiz. 64, 1734 (1973) [Sov. Phys.-JETP 37, 875 (1973)].
[7]Y. Matsumoto, T. Sakai, and S. Mase, J. Phys. Soc. Jpn. 28, 1211 (1970).
[8]A. P. Korolyuk, Zh. Eksp. Teor. Fiz. 49, 1009 (1965) [Sov. Phys.-JETP 22, 701 (1966)].
[9]Y. Sawada and E. Burstein, Phys. Rev. 150, 456 (1966).
[10]R. Herman, S. Hess, and H. U. Muller, Phys. Status Solidi B 48, K151 (1971).
[11]M. S. Khaikin and V. S. Edel'man, Zh. Eksp. Teor. Fiz. 47, 878 (1964) [Sov. Phys.-JETP 20, 587 (1965)].
[12]R. N. Brown, J. G. Mavroides, and B. Lax, Phys. Rev. 129, 2055 (1963).
[13]M. Maltz and M. S. Dresselhaus, Phys. Rev. B 2, 2877 (1970).
[14]M. P. Vecchi and M. S. Dresselhaus, Phys. Rev. B 9, 2877 (1974).
[15]G. A. Williams, Phys. Rev. 139, A771 (1965).
[16]R. T. Isaacson and G. A. Williams, Phys. Rev. 177, 738 (1969).
[17]S. Takano and H. Kawamura, J. Phys. Soc. Jpn. 28, 348 (1970).
[18]M. H. Cohen, Phys. Rev. 121, 387 (1961).
[19]E. O. Kane, J. Phys. Chem. Solids 1, 249 (1957).
[20]T. W. Nee, T. F. Koch, and R. E. Prange, Phys. Rev. 174, 758 (1968).
[21]J. F. Koch and C. C. Kuo, Phys. Rev. 143, 470 (1966).
[22]J. F. Koch and J. D. Jensen, Phys. Rev. 184, 643 (1969).
[23]M. S. Khaikin, Zh. Eksp. Teor. Fiz. 55, 1696 (1968) [Sov. Phys.-JETP 28, 892 (1969)].
[24]R. J. Dinger and A. W. Lawson, Phys. Rev. B 3, 253 (1971).
[25]S. Golin, Phys. Rev. 166, 643 (1968).